Desalination and Water Treatment
www.deswater.com

doi: 10.5004/dwt.2017.21204

84 (2017) 215–224
July

The size and concentration effects of Al_2O_3 nanoparticles on PSF membranes with enhanced structural stability and filtration performance

Seda Saki[a], Nigmet Uzal[b,*], Nuray Ates[c]

[a]*Department of Advanced Materials and Nanotechnology, Abdullah Gül University, 38080 Kayseri, Turkey, Tel. +903522248800; Fax: +903523388828; email: seda.saki@agu.edu.tr*
[b]*Department of Civil Engineering, Abdullah Gül University, 38080 Kayseri, Turkey, Tel. +903522248800; Fax: +903523388828; email: nigmet.uzal@agu.edu.tr*
[c]*Department of Environmental Engineering, Erciyes University, 38039 Kayseri, Turkey, Tel.+90352207666; Fax: +903524375784; email: nuraya@erciyes.edu.tr*

Received 16 January 2017; Accepted 12 July 2017

ABSTRACT

Nanocomposite membranes have attracted attention for their high permeability, rejection efficiency, and thermal and mechanical stability. In this study, novel flat-sheet polysulfone nanocomposite membranes were prepared by a phase inversion method with polyethylenimine and Al_2O_3 nanoparticles to increase the flux and hydrophilicity. Al_2O_3 nanoparticles were added to the membrane matrix to enhance the permeability, selectivity, and mechanical resistance. Two different sizes of Al_2O_3 nanoparticles (20 and 80 nm) were used with different weight percentages of 0.2, 1, and 5 wt%. The effects of the size and concentration of the nanoparticles on the structural properties and filtration performance of the membranes were investigated. Scanning electron microscopy, Fourier transform infrared spectroscopy, porosity, water contact angle, thermogravimetric analysis, viscosity, and tensile strength measurements were used to characterize the prepared membranes. The membrane performance was evaluated with water flux and bovine serum albumin rejection tests. According to the results, the membrane containing 15 wt% polysulfone, 1 wt% polyethylenimine, and 5 wt% 20 nm Al_2O_3 showed the highest pure water flux, porosity, viscosity, and morphological stability. This membrane may have potential uses in water treatment applications.

Keywords: Al_2O_3 nanoparticles; Nanocomposite membrane; Phase inversion; Bovine serum albumin rejection

1. Introduction

Polysulfone (PSF) is widely used to fabricate membranes because of its mechanical robustness, structural and chemical stability, large range of solubility, and thermal resistance [1,2]. However, PSF membranes need to be modified to reduce their hydrophobic characteristics and increase their permeability and antifouling capacity [3–6]. To improve the membrane hydrophilicity for water-based separation applications, hydrophilic polymers can be added to the casting solution, such as polyvinylpyrrolidone (PVP), polyethylene glycol, and polyethylenimine (PEI) [7–10]. Among these additives, PEI is shown to be a favorable polymeric amine with special features, and it is mostly used as a macrovoid formation agent [11,12].

However, the addition of hydrophilic polymers, including PEI, can decrease the mechanical strength, stability, and selectivity of the membrane [13]. To overcome these problems, blending the polymer with inorganic nanoadditives has also become a popular approach for the design of new PSF membranes with desirable properties [14,15]. PSF membranes with inorganic nanoadditives have better permeability, selectivity, and mechanical strength than pure PSF membranes. The incorporation of nanoadditives in the polymer matrix also enhances the membrane's permeability,

* Corresponding author.

selectivity, tensile strength, and thermal and chemical resistance [16–19].

Many studies have examined metal oxide nanoadditives to provide immense changes in the performance of polymeric nanocomposite membranes. Examples include TiO_2 [20], Al_2O_3, ZrO_2 [21], SiO_2 [22], Fe_3O_4 [23], and silver [24]. Particularly, Al_2O_3 is one of the most suitable nanoadditives for altering the hydrophilicity and mechanical resistance, and it is non-toxic [25]. Hydrophilic Al_2O_3 nanoparticles exhibit desirable compatibility with a polymer matrix, controllable design, and minimal aggregation at different particle sizes and concentrations [26,27]. The use of inorganic nanoparticles in a membrane matrix could provide synergistic effects on the membrane performance [28–31].

Maximous et al. [1] investigated the effects of Al_2O_3 concentration on membrane permeability and fouling resistance. Their results showed that the membrane porosity and performance improved with the addition of Al_2O_3 nanoparticles. Yan et al. [32] studied the effect of 10 nm Al_2O_3 nanoparticles on the performance of polyvinylidene fluoride (PVDF) ultrafiltration membranes. They demonstrated that the addition of 2 wt% Al_2O_3 nanoparticles to the PVDF polymer matrix significantly improved the hydrophilicity, water flux, and mechanical stability of the membranes. Although an excessive amount of inorganic Al_2O_3 particles in the casting solution (3–4 wt%) caused the membrane elasticity and flux to decline, it did not affect the hydrophilicity and porosity.

Mollahosseini et al. [33] investigated the influence of the size of nanoparticles in a casting solution with two different sizes of silver nanoparticles. They used 30 and 70 nm silver nanoparticles in a PSF/PVP matrix. Their results showed that the 30 nm particle size provided a more hydrophilic surface, higher water fluxes, and higher bovine serum albumin (BSA) rejection.

This study focuses on fabricating PSF/PEI nanocomposite membranes using two different particle sizes of Al_2O_3 nanoparticles (20 and 80 nm) via the phase inversion method. To the best of our knowledge, there are no reported data on using a PSF/PEI/Al_2O_3 blended substrate to fabricate polymeric nanocomposite membranes, and the effect of the Al_2O_3 nanoparticle size on PSF/PEI membranes has not been examined. The effects of the nanoparticle size and concentration on the performance of membranes were thus investigated. The membrane properties were evaluated by scanning electron microscopy (SEM), Fourier transform infrared spectroscopy (FTIR), contact angle, porosity, water flux, thermogravimetric analysis (TGA), BSA rejection, tensile strength, and viscosity measurements. The findings provide new insight that may contribute to the development of better nanocomposite membranes for water-based filtration applications.

2. Experimental

2.1. Materials

PSF with a weight-average molecular weight of 60,000 was purchased from Acros Organics, Belgium. An aqueous solution of branched PEI with a number-average molecular weight of 10,000 and a weight-average molecular weight of 25,000 was obtained from Sigma-Aldrich (USA) and used as a modifying agent. *N*,*N*-Dimethylformamide (DMF; Merck (USA), anhydrous, 99.8%) and 1-methyl-2-pyrrolidinone (NMP, Merck) were used as solvents. Hydrophilic Al_2O_3 nanoparticles with sizes of 20 and 80 nm were supplied from Nanografi, Turkey, and used as additives for the PSF/PEI solutions. BSA was used as a foulant and supplied from Amresco Inc. (USA). All of the organic and inorganic reagents were of analytical grade and used as received.

2.2. Preparation of membranes

For the fabrication of the membranes, the 20 and 80 nm and Al_2O_3 were first dissolved in an NMP solution at three different concentrations of 0.2, 1, and 5 wt% Al_2O_3 to reduce agglomeration. The mixture was then sonicated for 2 h. Next, the Al_2O_3 mixture was added to another mixture containing 15 wt% PSF and 1 wt% PEI polymer in DMF and NMP. The final solution was mixed for 1 d at 400 rpm using a magnetic stirrer to make it homogeneous. The polymer suspension was then sonicated for at least 2 h at 25°C. The details of the casting solution compositions are shown in Table 1. All casting solutions were allowed to stand for 1 h to remove all air bubbles, and then they were cast onto a clean glass plate (20–30 cm) with a steel casting knife. The fixed thickness of the cast film was 350 ± 20 μm. The film was immediately immersed in a distilled water bath for 2 min to remove the residual solvents and for solidification. All prepared membranes were stored in a bottle of deionized (DI) water at 4°C.

2.3. Characterization

2.3.1. SEM

The top-surface and cross-section morphologies of the membranes were observed using a Zeiss Leo 440 scanning electron microscope. The membranes were carefully sectioned with an approximate length of 3 mm and width of 0.5 mm using sharp scissors and then mounted onto the SEM grid. Prior to the examination, each sample was coated with platinum, and the samples were analyzed at 10 kV.

2.3.2. Water contact angle

The surface hydrophilicity of the membranes was measured using a contact angle meter (Attension-Theta Lite, Biolin Scientific, Finland). DI water was used to compare the hydrophilicity of the pure PSF, PSF/PEI, and PSF/PEI/Al_2O_3 membranes. For each measurement, at least three readings from different surface locations were taken, and the reported

Table 1
Casting solution compositions of membranes

Substrate	PSF (wt%)	PEI (wt%)	20 nm Al_2O_3 (wt%)	80 nm Al_2O_3 (wt%)
M201	15	1	0.2	–
M202	15	1	1	–
M203	15	1	5	–
M801	15	1	–	0.2
M802	15	1	–	1
M803	15	1	–	5

contact angles are the average values. All of the membranes were fully dried before measuring the contact angle to avoid issues with water interaction.

2.3.3. Water filtration test

A dead-end stirred cell filtration system (Sterlitech, HP4750) was used to determine the membranes' intrinsic separation properties (i.e., water permeability and rejection). The effective membrane area for the system was 14.6 cm^2. In the water filtration test, three different transmembrane pressures (TMP) were applied (0.2, 0.4, and 0.6 MPa), and the temperature was kept at room temperature (25°C ± 3°C). The water fluxes of the prepared membranes were calculated using Eq. (1):

$$J = \frac{\mathrm{V}}{\mathrm{A} \times \mathrm{t}} \tag{1}$$

where J is the water flux (L/m^2 h), V is the permeate volume (L), A is the effective membrane area (m^2), and t is time (h).

2.3.4. BSA rejection

The membranes' BSA rejection performance was determined using aqueous solutions containing 2.5 g/L of BSA [34]. The solutions were prepared using DI water at room temperature. The experiments were carried out at 0.2 MPa TMP in the dead-end filtration setup, and the BSA concentrations were analyzed using UV–visible spectroscopy (UV-1800, Shimadzu, China). The BSA rejections (R) were calculated by Eq. (2):

$$\%R = 1 - \frac{C_p}{C_f} \times 100 \tag{2}$$

where C_p is the concentration of BSA in the permeate, and C_f is the concentration in the feed solution. The volume reduction ratio (VRR) is calculated using the following formula:

$$\mathrm{VRR} = \frac{V_0}{V_R} \tag{3}$$

where V_0 and V_R are the initial feed volume and retentate volume, respectively.

2.3.5. Porosity

For the porosity measurements, dry membranes were immersed in ethanol for 2 h, and the liquid on the surfaces of the membranes was removed using filter paper after removing them from the ethanol. The membrane porosity (ε) was calculated using Eq. (4) [35]:

$$\varepsilon = \frac{(\omega 1 - \omega 2)/\mathrm{d}\omega}{\frac{\omega 1 - \omega 2}{\mathrm{d}\omega} + \omega 2/\mathrm{dp}} \tag{4}$$

where ω_1 is the weight of the wet membrane (g), ω_2 is the weight of the dry membrane (g), dω is the density of pure water (0.998 g/cm^3), and dp is the polymer density (1.24 g/cm^3).

2.3.6. Fourier transform infrared spectroscopy

FTIR spectra were employed for functional identification of PEI and Al_2O_3 nanoparticles using an FTIR spectrometer (Thermo Nicolet Avatar 370). Prior to the FTIR measurements, the samples were dried in a drying oven for 15 min at 120°C.

2.3.7. Mechanical strength

The mechanical strength of the prepared membranes was measured using an AGS-J tensile testing machine (Shimadzu, Japan). The measurements were carried out according to the ASTM D 882 standard by applying a 500-N load at a crosshead speed of 1 mm/min. All the samples were cut into rectangles with dimensions of 6 × 2 cm^2 and vertically mounted between the two mechanical gripping units of the tester, leaving a 2-cm gauge length for mechanical loading. The sample thicknesses were measured with an electronic micrometer with ±0.1 μm precision (No. 293-561, Mitutoyo, Japan). The average values of mechanical strength were obtained from the results of three measurements.

2.3.8. Viscosity measurement

The average viscosity of the casting solutions were measured with a Rapid Visco Analyzer (Pertem, RVA 4500). The viscosity was measured at room temperature (25°C ± 3°C). To ensure complete uniformity of the samples to be analyzed, the rotation of the RVA was set to 60 rpm for 120 s.

2.3.9. Thermal stability

The thermal stability of the membranes was determined by TGA (DTG-60H, Shimadzu). In order to remove the residual solvent from the membranes, 5–10 mg membrane samples were kept at 50°C for 12 h under vacuum and then heated under N_2 atmosphere from 30°C to 700°C at 10°C/min.

3. Results and discussion

PSF/PEI membranes were fabricated using two different particle sizes of Al_2O_3 at different concentrations in a membrane matrix. The following results first describe the changes in the solution viscosity and membrane structural morphology as a result of Al_2O_3 incorporation. Next, the changes to the membrane porosity are presented, followed by the water fluxes and BSA rejections and the effects of the Al_2O_3 on the membrane performance.

3.1. Viscosity test

Viscosity is one of the most important parameters for membrane fabrication because it affects the solvent and non-solvent exchange rate and the final morphology of the formed membranes [36]. Fig. 1 shows viscosity values of the casting solutions used to prepare the membranes. The results show that the addition of PEI and Al_2O_3 increased the viscosity of all solutions with increasing Al_2O_3 ratio for both sizes of nanoparticles. The addition of 1 wt% PEI increased the viscosity from 170 to 278 Cp. As shown in Fig. 1, increasing the

Al_2O_3 concentration also increased the viscosity from 320 to 540 Cp and from 265 to 495 Cp for the 20 and 80 nm particles, respectively.

The highest viscosity was obtained from the PSF/PEI solution containing 5 wt% 20 nm Al_2O_3 nanoparticles. This result can be explained in terms of the adsorption between the polymeric chains and the exposed hydroxyl groups at the surface of the nanoparticles, which have high specific surface area and surface energy [37,38]. White and Crowder [39] and Taurozzi et al. [40] also reported an increase in the viscosity of the solution when the loading of nanoparticles was higher and when the nanoparticles were smaller at the same nanoparticle loading. The effects of the nanoparticle loading and size were attributed to the change in the relaxation modulus and the elastic recovery of the mixture. The results were also correlated to changes in the available polymer–nanoparticle interfacial surface area, which is affected by both the loading and the size of the TiO_2 nanoparticles [38].

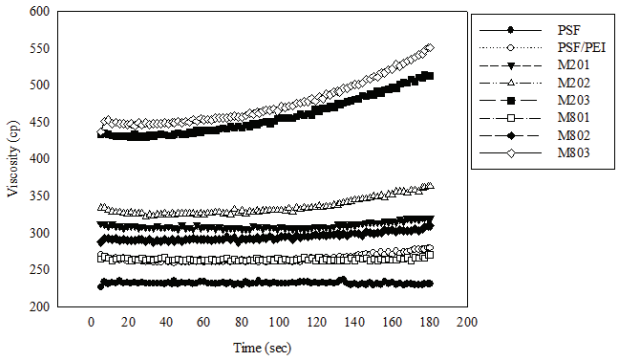

Fig. 1. Viscosity values of the casting solutions for the PSF, PSF/PEI, and PSF/PEI/Al_2O_3 nanocomposite membranes.

3.2. Membrane morphology

Morphology analysis is another very important tool for the development of membranes. To investigate the morphological changes associated with the addition of PEI and Al_2O_3, images of the top and cross-sections of the membranes were obtained by SEM. The morphology is influenced by various factors, including the interaction, viscosity, and diffusion rate of casting solution [41]. The rates of solidification and coagulation of PSF polymer determine the membrane matrix formation [42].

Images of the membrane surfaces and cross-sections are shown in Fig. 2. As shown in Fig. 2(a), a uniform surface without nodules was formed during the fabrication of the pure PSF membrane. However, the surface was completely different and had small pores when PEI was added to the polymer matrix (Fig. 2(b)). The PSF membrane exhibited a

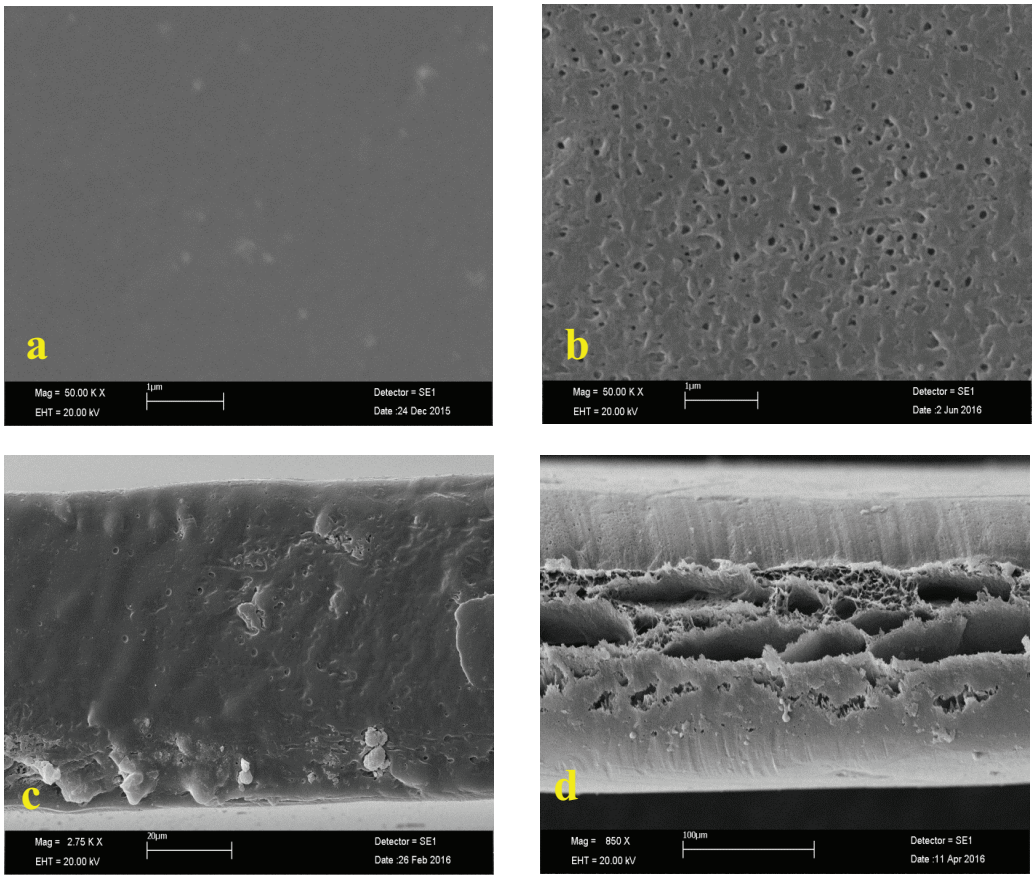

Fig. 2. SEM images of PSF and PSF/PEI membranes: (a) PSF surface, (b) PSF/PEI surface, (c) PSF cross-section, and (d) PSF/PEI cross-section.

very dense structure and few macrovoids, which results in mechanical support. During the phase inversion process, the fast solvent and non-solvent exchange occurs, and repulsive forces between PSF and water cause immediate precipitation on the polymer structure (Fig. 2(c)) [43,44]. The addition of PEI to the polymer matrix results in the formation of an asymmetric structure consisting of a thin and dense top layer and a finger-like macroviod structure at the bottom layer (Fig. 2(d)) [45].

Cross-section images of the PSF/PEI membranes with different concentrations of 20 nm Al_2O_3 (0.2, 1, and 5 wt%) are shown in Fig. 3. The membrane morphology changed significantly with the nanoparticle concentration. Compared with the pure PSF membrane (Fig. 2(c)), the Al_2O_3 nanoparticles result in the development of a long finger-like structure in the cross-section. With increasing content of Al_2O_3, the amount of finger-like pores increased, and the clear boundary between the sublayer and center of the membrane disappeared with the addition of 5 wt% Al_2O_3 (Fig. 3(c)) [46].

Fig. 4 shows compares the cross-section SEM images of the 20 and 80 nm Al_2O_3 at 5 wt%. The 20 nm Al_2O_3 was dispersed uniformly in the polymer matrix (Fig. 4(a)), but the 80 nm Al_2O_3 membrane had many short finger-like structures in the center, which were covered with dense top and bottom layers. This is attributed to the high loading amount resulting in unstable distribution in the PSF/PEI membrane matrix (Fig. 4(b)) [47]. This could be explained by the high viscosity of the casting solution when the 20 nm Al_2O_3 is added, as well as the high affinity of the 20 nm nanoparticles to the polymeric phase [48].

3.3. Porosity

In general, membrane porosity is dependent on the mass transfer of the casting solution during the phase inversion process [49]. The hydrophilic functional groups from the nanoparticles speed up the membrane formation process by accelerating the exchange rate between the solvent and non-solvent. Consequently, the pore formation process would be enhanced. As shown in Table 2, the porosity of membranes increased from 63% for the pure PSF membrane to 79% and 65% for membranes with 5 wt% 20 and 80 nm Al_2O_3 nanoparticles, respectively. All the blended membranes showed improved porosity, but there was a small decrease for the 80 nm Al_2O_3 at 5 wt%. This might have been caused by pore blockage due to the high particle size and amount of Al_2O_3 [50].

The improvements of the porosity of the nanocomposite membranes were attributed to the lower viscosity of the blending solution with the addition of hydrophilic Al_2O_3, which led to a faster occurrence of the phase inversion process [51]. These results may be explained by the retarded solution demixing and improved kinetic hindrance, which increased the viscosity. The increased viscosity supports the diffusion of solvent from the solution over the internal diffusion of non-solvent into the cast membrane, resulting in lower porosity [45,52,53]. This result is also in agreement with findings by Choi et al. [54], who prepared nanocomposite UF membranes from PSF casting solutions loaded with different amounts of multi-walled carbon nanotubes (CNTs).

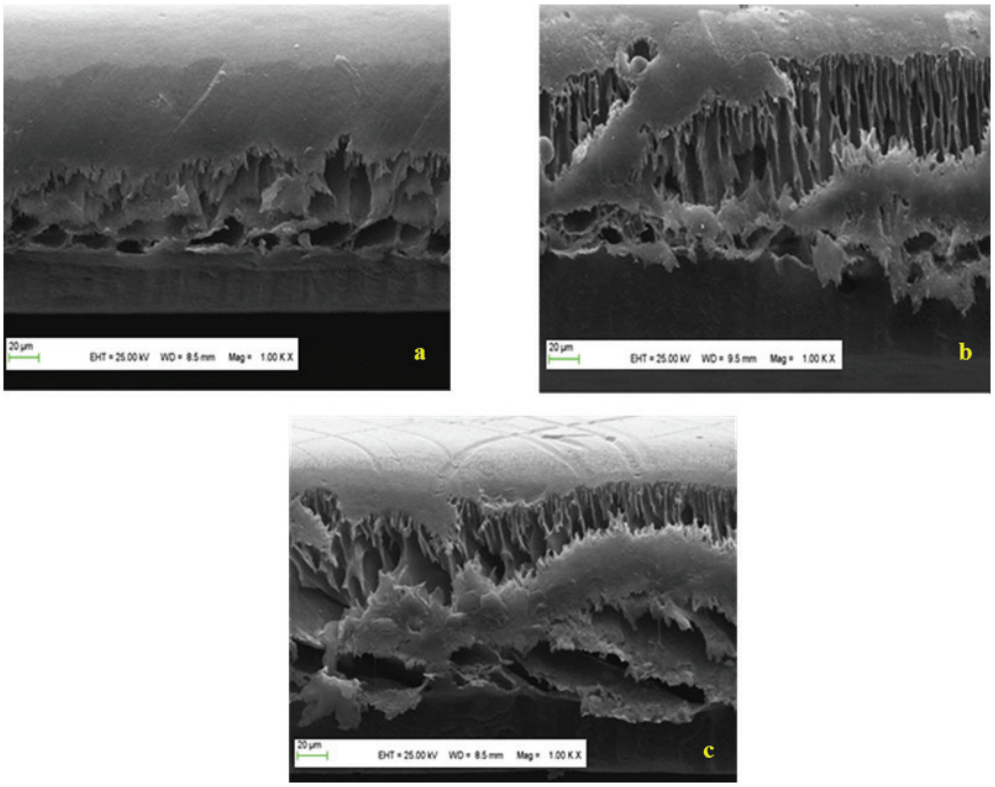

Fig. 3. SEM images of PSF/PEI membranes cross-section containing 20 nm Al_2O_3 with different concentrations: (a) 0.2 wt%, (b) 1 wt%, and (c) 5 wt%.

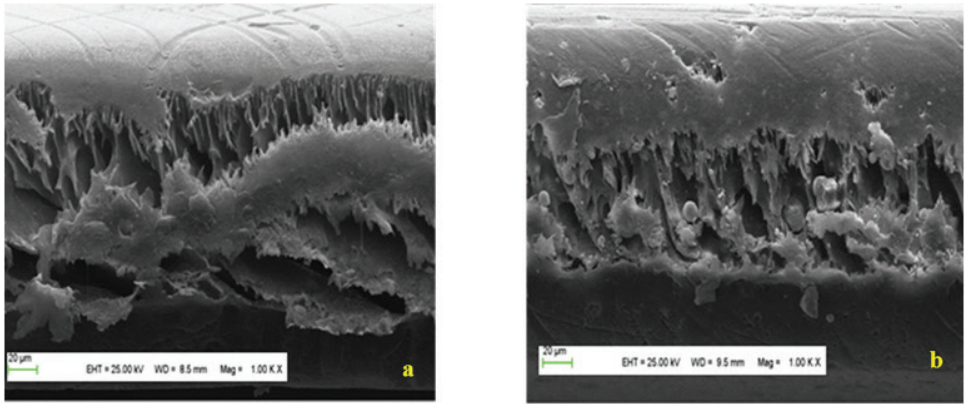

Fig. 4. Cross-section SEM images of PSF/PEI membrane containing 5 wt% Al_2O_3 nanoparticles: (a) 20 nm Al_2O_3 and (b) 80 nm Al_2O_3.

Table 2
Contact angle, pure water flux (at 0.4 MPa), and porosity of PSF, PSF/PEI, PSF/PEI/Al_2O_3 nanocomposite membranes

Substrate	CA (°)	Water flux (L/m^2 h)	Porosity (%)
PSF	87 ± 2	20.51	63 ± 3
PSF/PEI	64 ± 4	317.70	95 ± 4
M201	72 ± 5	236.02	71 ± 2
M202	65 ± 2	1,289.12	77 ± 5
M203	56 ± 3	1,336.6	79 ± 6
M801	81 ± 6	103.16	68 ± 3
M802	77 ± 3	1,027.05	73 ± 2
M803	55 ± 2	901.35	65 ± 4

3.4. Membrane hydrophilicity

The hydrophilicity of the nanocomposite membranes was evaluated by the contact angle using the sessile drop method, as shown in Table 2. The pure PSF membrane's contact angle was 87°, but PEI addition decreased the contact angle to 67°. The contact angles were 72°, 65°, and 56° for membranes with 20 nm Al_2O_3 nanoparticles at 0.2, 1, and 5 wt% loading, respectively. For 80 nm Al_2O_3 nanoparticles, the contact angles were 81°, 77°, and 55° for 0.2, 1, and 5 wt% loadings, respectively. The contact angles of the PSF/PEI nanocomposite membranes were lower for 0.2 wt% concentration at both sizes of Al_2O_3 nanoparticles. When the amount was increased 0.2–5 wt%, the contact angles decreased for both sizes. This could be due to greater migration of nanoparticles to the surface during the phase inversion process at high concentration [52,55]. The membrane hydrophilicity was positively affected by increasing the nanoparticle loading, but the particle size had no significant effect.

3.5. Mechanical properties

Adding the nanoparticles improved the morphological and structural parameters of the membrane, as well as the mechanical resistance. The tensile strength of the membranes is shown in Fig. 5. The tensile strength of the pure PSF membrane was 3.18 MPa, which decreased to 3.02 MPa with the addition of PEI due to the increased pore formation [56]. Incorporating 0.2, 1, and 5 wt% 20 nm Al_2O_3 nanoparticles

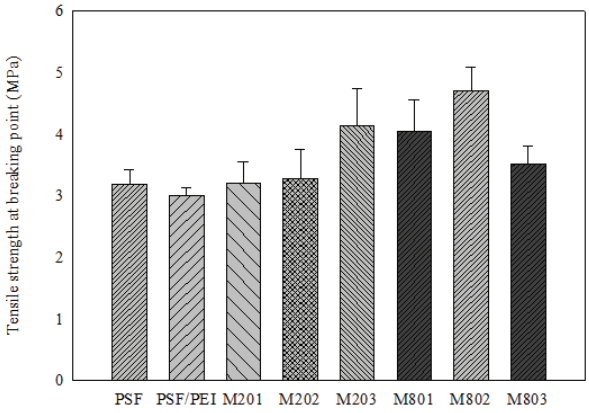

Fig. 5. Tensile strength of breaking point of PSF, PSF/PEI, and PSF/PEI/Al_2O_3 nanocomposite membranes.

increased the tensile strength to 3.2, 3.7, and 4.1 MPa, respectively. This could be explained by the interaction between the nanoparticles and the PSF/PEI matrix. Al_2O_3 could act as a cross-linking point to connect the polymer chains and increase their rigidity. Therefore, more energy would be needed to break down the bonds between the Al_2O_3 and PSF, and the tensile strength was improved [57]. With increasing amount of Al_2O_3, the tensile strength values increased slightly. As shown in Fig. 5, the tensile strength with 0.2 and 1 wt% 80 nm Al_2O_3 first increased and then declined at 5 wt% Al_2O_3.

When adding 5 wt% 80 nm Al_2O_3, the tensile strength decreased from 4.7 to 3.2 MPa. Excessive concentration may cause nanoparticle aggregation and decrease the tensile strength. Kumar et al. [58] prepared a PSF membrane containing graphene oxide (GO)–TiO_2 nanoparticles by a blending method. They found that the tensile strength was enhanced with lower amounts of GO–TiO_2 of up to 2 wt%, but it decreased when the loading was further increased to 3–5 wt%.

3.6. Thermal stability

The thermal stabilities of the membranes were measured by TGA, as shown in Fig. 6. The thermal decomposition temperatures were in the range of 500°C–550°C. The TGA

measurement results confirmed that PSF is a thermally stable polymer due to its fully aromatic structure [59]. As shown in the TGA curves, the nanoparticles have no significant effect on the thermal decomposition temperature.

3.7. Fourier transform infrared spectroscopy

The surface functional groups and chemical composition of the membranes were determined by FTIR, as shown in Fig. 7. The characteristic absorption peaks of PSF were around 1,149 and 1,168 cm^{-1} (SO_2 symmetrical stretching), 1,244 cm^{-1} (aryl-O-aryl C–O stretching), 1,582 cm^{-1} (SO_2 asymmetric stretching), 1,677 cm^{-1} (asymmetric–CH_3), and 2,151 cm^{-1} (C=C) [60,61]. A new peak occurred at 3,700 cm^{-1} in the spectrum of Al_2O_3 nanoparticle membranes, which is related to the –OH and Al–O functional groups of the Al_2O_3 nanoparticles [46]. This can be attributed to the successful interaction between the base polymer and inorganic phases. All of the membranes also had the same basic structure of PSF. Comparison between the spectrum of the PSF membrane and nanocomposite membrane showed a similar PSF characteristic peak in the area of 1,000–3,500 cm^{-1} because of the high PSF concentration. Thus, it is assumed that the membrane was successfully modified based on the higher peak obtained.

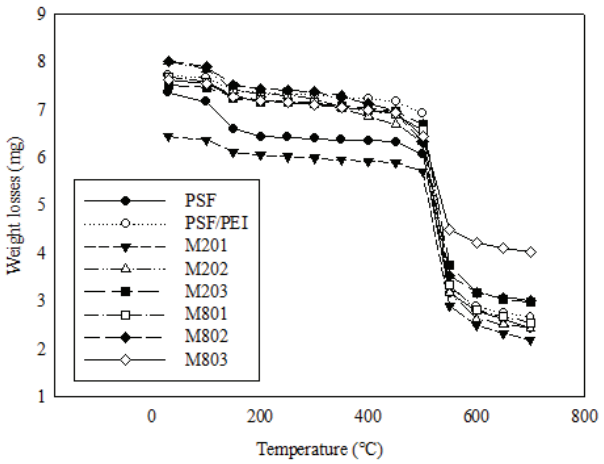

Fig. 6. TGA curves of PSF, PSF/PEI, and PSF/PEI/Al_2O_3 nanocomposite membranes.

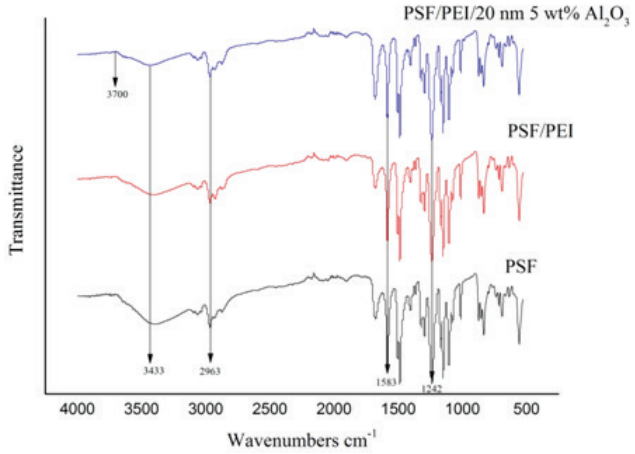

Fig. 7. FTIR spectrum of PSF, PSF/PEI, and PSF/PEI membrane containing 5 wt% Al_2O_3.

3.8. Filtration properties

3.8.1. Pure water flux

The water fluxes of the membranes were determined at three different pressures (0.2, 0.4, and 0.6 MPa), as shown in Fig. 8. The pure PSF membrane showed the lowest water flux of 20.51 L/m^2 h at 0.4 MPa, and the highest water flux was obtained for the membranes with 5 wt% 20 nm Al_2O_3 nanoparticles as 1,336.6 L/m^2 h at 0.4 MPa. This result could be explained by the Al_2O_3 enhancing the hydrophilicity (Table 2) and porosity compared with the pure PSF membranes [62,63].

Although increasing the amount of 20 nm Al_2O_3 nanoparticles enhanced the water flux of membranes, increasing the amount of 80 nm nanoparticles to 5 wt% adversely affected the water flux of membranes. This might be a result of pore blockage by the large nanoparticles [15,33]. Therefore, either agglomeration or the slower exchange of solvent and non-solvent could not be prevented during the phase inversion process [63,64].

These findings also might be supported by the porosity data. Higher porosity results in higher water flux values [65,66]. Esfahani et al. [67] reported that the pure water flux was increased from 10 to 210 L/m^2 h at 0.16 MPa by incorporation of 1 wt% multi-walled CNTs. In our study, the pure water flux increased from 20.51 to 700.2 L/m^2 h at 0.2 MPa by incorporation of 1 wt% Al_2O_3 (20 nm). Moreover, when the Al_2O_3 nanoparticle concentration increased to 5 wt%, the water flux increased to 850.2 L/m^2 h at 0.2 MPa TMP. These results demonstrate that the Al_2O_3 nanoparticles have a more remarkable effect on the pure water flux than multi-walled CNTs.

3.8.2. BSA rejection

BSA filtration experiments were carried out using the same system described in section 3.8.1. A 2.5 g/L BSA solution

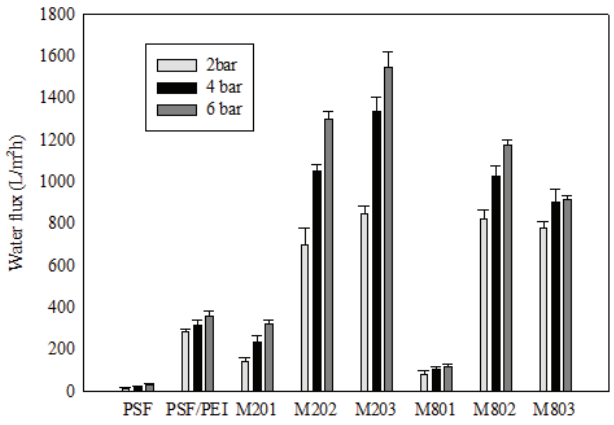

Fig. 8. Water fluxes of PSF, PSF/PEI, and PSF/PEI/Al_2O_3 nanocomposite membranes at different pressures.

was used because of its hydrophobic nature and appropriate molecular size to evaluate the separation performance. Fig. 9 shows the BSA rejection performance results. The BSA rejection values of the pure PSF and PSF/PEI membranes were 83% and 72%, respectively. The PSF/PEI membrane had the lowest BSA rejection because of its higher porosity and consequently lower selectivity [68]. All of the prepared PSF/PEI/Al_2O_3 nanocomposite membranes rejected more than 90% of the BSA protein. The results are better than those obtained by Nair et al. [69], who achieved maximum BSA rejections of 88%–94% using PSF membranes with $CaCO_3$ nanoparticles.

Fig. 10 shows the variation of the BSA flux vs. VRR at an operating pressure of 2 bar. The membranes with 5 and 1 wt% 20 nm Al_2O_3 showed the highest flux values.

4. Conclusions

PSF-based nanocomposite membranes were prepared by the incorporation of PEI and two different sizes of Al_2O_3 nanoparticles at different concentrations via the phase inversion method. The hydrophilicity, porosity, viscosity, water flux, and tensile strength were enhanced as the Al_2O_3 content increased. The hydrophilic and porous structure of the Al_2O_3 had a strong impact on the membranes properties. The PSF/PEI/Al_2O_3 membranes with 5 wt% 20 nm Al_2O_3 nanoparticles showed excellent water flux of 1,336.6 L/m^2 h at 0.4 MPa, as well as a contact angle of 56°, porosity of 79%, and tensile strength of 4.1 MPa.

The smaller Al_2O_3 nanoparticles produced better water flux, porosity, morphological stability, and tensile strength because of the high surface area and the higher water adsorption capacity. When increasing the concentration of 80 nm Al_2O_3 nanoparticles to 5 wt%, aggregation problems occurred, and water flux, porosity, and tensile strength declined. However, with 20 nm Al_2O_3 nanoparticles, this problem was not observed.

The nanocomposite membranes with 5 wt% 80 nm nanoparticles showed the highest BSA rejection of 99%, but with 20 nm particles, the rejection values decreased slightly to about 96%. All of the nanocomposite membranes exhibited ultrafiltration membrane characteristics with over 90% rejection rates. Although the water flux, porosity, and tensile strength were positively affected by increasing the nanoparticle concentration, the particle size had no significant effect on the membrane hydrophilicity and thermal resistance. The hydrophilicity and mechanical properties indicate that the PSF/PEI/Al_2O_3 nanocomposite membranes could be significant candidates for water and wastewater treatment applications.

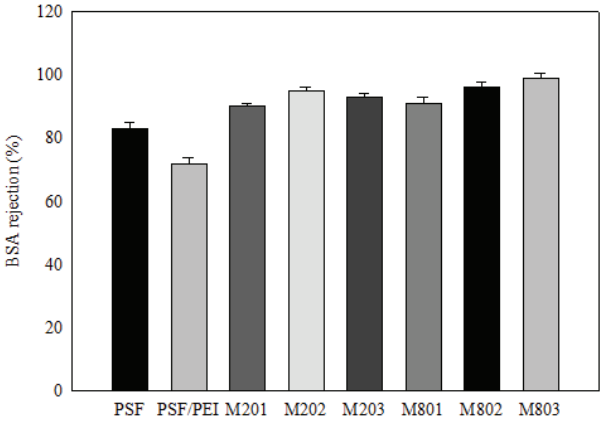

Fig. 9. BSA rejection performance of PSF, PSF/PEI, and PSF/PEI/Al_2O_3 nanocomposite membranes.

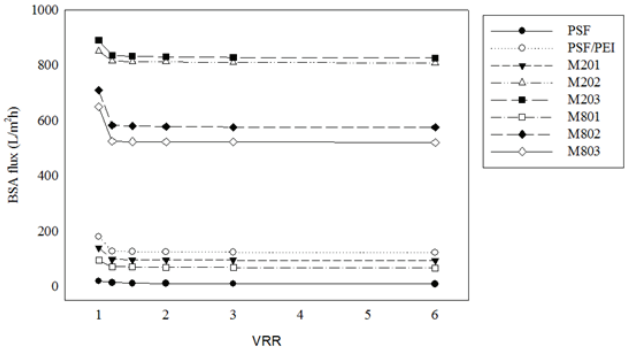

Fig. 10. BSA rejection performance of PSF, PSF/PEI, and PSF/PEI/Al_2O_3 nanocomposite membranes.

Acknowledgment

The authors extend their appreciation to the Scientific Research Foundation of Abdullah Gül University (Project No. FYL-2016-75) for funding this study.

References

[1] N. Maximous, G. Nakhla, W. Wan, K. Wong, Preparation, characterization and performance of Al_2O_3/PES membrane for wastewater filtration, J. Membr. Sci., 341 (2009) 67–75.
[2] M.Z. Yunos, Z. Harun, H. Basri, A.F. Ismail, Studies on fouling by natural organic matter (NOM) on polysulfone membranes: effect of polyethylene glycol (PEG), Desalination, 333 (2014) 36–44.
[3] X.-Y. Li, H.P. Chu, Membrane bioreactor for the drinking water treatment of polluted surface water supplies, Water Res., 37 (2003) 4781–4791.
[4] A. Fenu, G. Guglielmi, J. Jimenez, M. Spèrandio, D. Saroj, B. Lesjean, C. Brepols, C. Thoeye, I. Nopens, Activated sludge model (ASM) based modelling of membrane bioreactor (MBR) processes: a critical review with special regard to MBR specificities, Water Res., 44 (2010) 4272–4294.
[5] R. van Reis, A. Zydney, Bioprocess membrane technology, J. Membr. Sci., 297 (2007) 16–50.
[6] R. Kumar, A.M. Isloor, A.F. Ismail, S.A. Rashid, A.A. Ahmed, Permeation, antifouling and desalination performance of TiO_2 nanotube incorporated PSf/CS blend membranes, Desalination, 316 (2013) 76–84.
[7] J. Garcia-Ivars, M.-I. Alcaina-Miranda, M.-I. Iborra-Clar, J.-A. Mendoza-Roca, L. Pastor-Alcañiz, Enhancement in hydrophilicity of different polymer phase-inversion ultrafiltration membranes by introducing PEG/Al_2O_3 nanoparticles, Sep. Purif. Technol., 128 (2014) 45–57.
[8] R. Kumar, A.M. Isloor, A.F. Ismail, T. Matsuura, Performance improvement of polysulfone ultrafiltration membrane using N-succinyl chitosan as additive, Desalination, 318 (2013) 1–8.
[9] H. Susanto, M. Ulbricht, Characteristics, performance and stability of polyethersulfone ultrafiltration membranes prepared by phase separation method using different macromolecular additives, J. Membr. Sci., 327 (2009) 125–135.
[10] Y. Ma, F. Shi, J. Ma, M. Wu, J. Zhang, C. Gao, Effect of PEG additive on the morphology and performance of polysulfone ultrafiltration membranes, Desalination, 272 (2011) 51–58.

[11] D. Wu, Y. Huang, S. Yu, D. Lawless, X. Feng, Thin film composite nanofiltration membranes assembled layer-by-layer via interfacial polymerization from polyethylenimine and trimesoyl chloride, J. Membr. Sci., 472 (2014) 141–153.
[12] S.-J. Park, R.K. Cheedrala, M.S. Diallo, C. Kim, I.S. Kim, W.A. Goddard, Nanofiltration membranes based on polyvinylidene fluoride nanofibrous scaffolds and crosslinked polyethyleneimine networks, J. Nanopart. Res., 14 (2012) 884.
[13] C. Ba, J. Langer, J. Economy, Chemical modification of P84 copolyimide membranes by polyethylenimine for nanofiltration, J. Membr. Sci., 327 (2009) 49–58.
[14] G. Zhang, S. Lu, L. Zhang, Q. Meng, C. Shen, J. Zhang, Novel polysulfone hybrid ultrafiltration membrane prepared with TiO_2-g-HEMA and its antifouling characteristics, J. Membr. Sci., 436 (2013) 163–173.
[15] M. Sianipar, S.H. Kim, C. Min, L.D. Tijing, H.K. Shon, Potential and performance of a polydopamine-coated multiwalled carbon nanotube/polysulfone nanocomposite membrane for ultrafiltration application, J. Ind. Eng. Chem., 34 (2016) 364–373.
[16] M.K. Sinha, M.K. Purkait, Increase in hydrophilicity of polysulfone membrane using polyethylene glycol methyl ether, J. Membr. Sci., 437 (2013) 7–16.
[17] A. Sotto, A. Boromand, R. Zhang, P. Luis, J.M. Arsuaga, J. Kim, B. Van der Bruggen, Effect of nanoparticle aggregation at low concentrations of TiO_2 on the hydrophilicity, morphology, and fouling resistance of PES–TiO_2 membranes, J. Colloid Interface Sci., 363 (2011) 540–550.
[18] T.A. Saleh, V.K. Gupta, Synthesis and characterization of alumina nano-particles polyamide membrane with enhanced flux rejection performance, Sep. Purif. Technol., 89 (2012) 245–251.
[19] M. Baghbanzadeh, D. Rana, C.Q. Lan, T. Matsuura, Effects of inorganic nano-additives on properties and performance of polymeric membranes in water treatment, Sep. Purif. Rev., 45 (2016) 141–167.
[20] A.K. Nair, P.M. Shalin, P.E. Jagadeesh Babu, Performance enhancement of polysulfone ultrafiltration membrane using TiO_2 nanofibers, Desal. Wat. Treat., 57 (2016) 10506–10514.
[21] A. Bottino, G. Capannelli, A. Comite, Preparation and characterization of novel porous PVDF-ZrO_2 composite membranes, Desalination, 146 (2002) 35–40.
[22] L.-Y. Yu, Z.-L. Xu, H.-M. Shen, H. Yang, Preparation and characterization of PVDF–SiO_2 composite hollow fiber UF membrane by sol–gel method, J. Membr. Sci., 337 (2009) 257–265.
[23] Z.-Q. Huang, K. Chen, S.-N. Li, X.-T. Yin, Z. Zhang, H.-T. Xu, Effect of ferrosoferric oxide content on the performances of polysulfone–ferrosoferric oxide ultrafiltration membranes, J. Membr. Sci., 315 (2008) 164–171.
[24] X. Liu, S. Qi, Y. Li, L. Yang, B. Cao, C.Y. Tang, Synthesis and characterization of novel antibacterial silver nanocomposite nanofiltration and forward osmosis membranes based on layer-by-layer assembly, Water Res., 47 (2013) 3081–3092.
[25] M. Homayoonfal, M.R. Mehrnia, Y.M. Mojtahedi, A.F. Ismail, Effect of metal and metal oxide nanoparticle impregnation route on structure and liquid filtration performance of polymeric nanocomposite membranes: a comprehensive review, Desal. Wat. Treat., 51 (2013) 3295–3316.
[26] A. Rahimpour, M. Jahanshahi, S. Khalili, A. Mollahosseini, A. Zirepour, B. Rajaeian, Novel functionalized carbon nanotubes for improving the surface properties and performance of polyethersulfone (PES) membrane, Desalination, 286 (2012) 99–107.
[27] X. Cao, J. Ma, X. Shi, Z. Ren, Effect of TiO_2 nanoparticle size on the performance of PVDF membrane, Appl. Surf. Sci., 253 (2006) 2003–2010.
[28] J. Vanneste, A. Sotto, C.M. Courtin, V. Van Craeyveld, K. Bernaerts, J. Van Impe, J. Vandeur, S. Taes, B. Van der Bruggen, Application of tailor-made membranes in a multi-stage process for the purification of sweeteners from *Stevia rebaudiana*, J. Food Eng., 103 (2011) 285–293.
[29] A. Rahimpour, M. Jahanshahi, B. Rajaeian, M. Rahimnejad, TiO_2 entrapped nano-composite PVDF/SPES membranes: preparation, characterization, antifouling and antibacterial properties, Desalination, 278 (2011) 343–353.
[30] S. Balta, A. Sotto, P. Luis, L. Benea, B. Van der Bruggen, J. Kim, A new outlook on membrane enhancement with nanoparticles: the alternative of ZnO, J. Membr. Sci., 389 (2012) 155–161.
[31] N. Maximous, G. Nakhla, W. Wan, K. Wong, Performance of a novel ZrO_2/PES membrane for wastewater filtration, J. Membr. Sci., 352 (2010) 222–230.
[32] L. Yan, Y.S. Li, C.B. Xiang, Preparation of poly(vinylidene fluoride)(pvdf) ultrafiltration membrane modified by nano-sized alumina (Al_2O_3) and its antifouling research, Polymer, 46 (2005) 7701–7706.
[33] A. Mollahosseini, A. Rahimpour, M. Jahamshahi, M. Peyravi, M. Khavarpour, The effect of silver nanoparticle size on performance and antibacteriality of polysulfone ultrafiltration membrane, Desalination, 306 (2012) 41–50.
[34] S. Jamal, S. Chang, H. Zhou, Filtration behaviour and fouling mechanisms of polysaccharides, Membranes, 4 (2014) 319–332.
[35] H. Lohokare, Y. Bhole, S. Taralkar, U. Kharul, Poly(acrylonitrile) based ultrafiltration membranes: optimization of preparation parameters, Desalination, 282 (2011) 46–53.
[36] A. Alpatova, E.-S. Kim, X. Sun, G. Hwang, Y. Liu, M.G. El-Din, Fabrication of porous polymeric nanocomposite membranes with enhanced anti-fouling properties: effect of casting composition, J. Membr. Sci., 444 (2013) 449–460.
[37] P. Aerts, E. Van Hoof, R. Leysen, I.F.J. Vankelecom, P.A. Jacobs, Polysulfone–Aerosil composite membranes: part 1. The influence of the addition of Aerosil on the formation process and membrane morphology, J. Membr. Sci., 176 (2000) 63–73.
[38] Y. Yang, H. Zhang, P. Wang, Q. Zheng, J. Li, The influence of nano-sized TiO_2 fillers on the morphologies and properties of PSF UF membrane, J. Membr. Sci., 288 (2007) 231–238.
[39] J.L. White, J.W. Crowder, The influence of carbon black on the extrusion characteristics and rheological properties of elastomers: polybutadiene and butadiene–styrene copolymer, J. Appl. Polym. Sci., 18 (1974) 1013–1038.
[40] J.S. Taurozzi, C.A. Crock, V.V. Tarabara, C60-polysulfone nanocomposite membranes: entropic and enthalpic determinants of C60 aggregation and its effects on membrane properties, Desalination, 269 (2011) 111–119.
[41] M. Alhoshan, J. Alam, L.A. Dass, N. Al-Homaidi, Fabrication of polysulfone/ZnO membrane: influence of ZnO nanoparticles on membrane characteristics, Adv. Polym. Tech., 32 (2013) 21369(1–7).
[42] S. Zhao, W. Yan, M. Shi, Z. Wang, J. Wang, S. Wang, Improving permeability and antifouling performance of polyethersulfone ultrafiltration membrane by incorporation of ZnO-DMF dispersion containing nano-ZnO and polyvinylpyrrolidone, J. Membr. Sci., 478 (2015) 105–116.
[43] H.B.T. Jeazet, C. Staudt, C. Janiak, A method for increasing permeability in O_2/N_2 separation with mixed-matrix membranes made of water-stable MIL-101 and polysulfone, Chem. Commun., 48 (2012) 2140–2142.
[44] P.V. Chai, E. Mahmoudi, Y.H. Teow, A.W. Mohammad, Preparation of novel polysulfone-Fe_3O_4/GO mixed-matrix membrane for humic acid rejection, J. Water Process Eng., 15 (2017) 83–88.
[45] I.M. Wienk, R.M. Boom, M.A.M. Beerlage, A.M.W. Bulte, C.A. Smolders, H. Strathmann, Recent advances in the formation of phase inversion membranes made from amorphous or semi-crystalline polymers, J. Membr. Sci., 113 (1996) 361–371.
[46] T.M. Costa, M.R. Gallas, E.V. Benvenutti, J.A. da Jornada, Study of nanocrystalline γ-Al_2O_3 produced by high-pressure compaction, J. Phys. Chem. B, 103 (1999) 4278–4284.
[47] V. Vatanpour, S.S. Madaeni, A.R. Khataee, E. Salehi, S. Zinadini, H.A. Monfared, TiO_2 embedded mixed matrix PES nanocomposite membranes: influence of different sizes and types of nanoparticles on antifouling and performance, Desalination, 292 (2012) 19–29.
[48] Z. Zhang, Q. An, Y. Ji, J. Qian, C. Gao, Effect of zero shear viscosity of the casting solution on the morphology and permeability of polysulfone membrane prepared via the phase-inversion process, Desalination, 260 (2010) 43–50.
[49] J. Hong, Y. He, Polyvinylidene fluoride ultrafiltration membrane blended with nano-ZnO particle for photo-catalysis self-cleaning, Desalination, 332 (2014) 67–75.

[50] R. Rezaee, S. Nasseri, A.H. Mahvi, R. Nabizadeh, S.A. Mousavi, A. Rashidi, A. Jafari, S. Nazmara, Fabrication and characterization of a polysulfone-graphene oxide nanocomposite membrane for arsenate rejection from water, J. Environ. Health, 13 (2015) 61.
[51] Y.T. Chung, M.M. Ba-Abbad, A.W. Mohammad, A. Benamor, Functionalization of zinc oxide (ZnO) nanoparticles and its effects on polysulfone-ZnO membranes, Desal. Wat. Treat., 57 (2016) 7801–7811.
[52] A. Khalid, A.A. Al-Juhani, O.C. Al-Hamouz, T. Laoui, Z. Khan, M.A. Atieh, Preparation and properties of nanocomposite polysulfone/multi-walled carbon nanotubes membranes for desalination, Desalination, 367 (2015) 134–144.
[53] M.-J. Han, S.-T. Nam, Thermodynamic and rheological variation in polysulfone solution by PVP and its effect in the preparation of phase inversion membrane, J. Membr. Sci., 202 (2002) 55–61.
[54] J.-H. Choi, J. Jegal, W.-N. Kim, Fabrication and characterization of multi-walled carbon nanotubes/polymer blend membranes, J. Membr. Sci., 284 (2006) 406–415.
[55] N. Meng, Z. Wang, Z.-X. Low, Y. Zhang, H. Wang, X. Zhang, Impact of trace graphene oxide in coagulation bath on morphology and performance of polysulfone ultrafiltration membrane, Sep. Purif. Technol., 147 (2015) 364–371.
[56] K. Wang, A.A. Abdalla, M.A. Khaleel, N. Hilal, M.K. Khraisheh, Mechanical properties of water desalination and wastewater treatment membranes, Desalination, 401 (2017) 190–205.
[57] M. Kumar, D. McGlade, M. Ulbricht, J. Lawler, Quaternized polysulfone and graphene oxide nanosheet derived low fouling novel positively charged hybrid ultrafiltration membranes for protein separation, RSC Adv., 5 (2015) 51208–51219.
[58] M. Kumar, Z. Gholamvand, A. Morrissey, K. Nolan, M. Ulbricht, J. Lawler, Preparation and characterization of low fouling novel hybrid ultrafiltration membranes based on the blends of GO–TiO_2 nanocomposite and polysulfone for humic acid removal, J. Membr. Sci., 506 (2016) 38–49.
[59] A. Ouradi, Q.T. Nguyen, A. Benaboura, Polysulfone–AN69 blend membranes and its surface modification by polyelectrolyte-layer deposit—preparation and characterization, J. Membr. Sci., 454 (2014) 20–35.
[60] A. Dehghani Kiadehi, A. Rahimpour, M. Jahanshahi, A.A. Ghoreyshi, Novel carbon nano-fibers (CNF)/polysulfone (PSf) mixed matrix membranes for gas separation, J. Ind. Eng. Chem., 22 (2015) 199–207.
[61] N.N. Rupiasih, H. Suyanto, M. Sumadiyasa, N. Wendri, Study of effects of low doses UV radiation on microporous polysulfone membranes in sterilization process, Open J. Org. Polym. Mater., 3 (2013) 12–18.
[62] E. Celik, L. Liu, H. Choi, Protein fouling behavior of carbon nanotube/polyethersulfone composite membranes during water filtration, Water Res., 45 (2011) 5287–5294.
[63] E.-S. Kim, G. Hwang, M. Gamal El-Din, Y. Liu, Development of nanosilver and multi-walled carbon nanotubes thin-film nanocomposite membrane for enhanced water treatment, J. Membr. Sci., 394–395 (2012) 37–48.
[64] S. Majeed, D. Fierro, K. Buhr, J. Wind, B. Du, A. Boschetti-de-Fierro, V. Abetz, Multi-walled carbon nanotubes (MWCNTs) mixed polyacrylonitrile (PAN) ultrafiltration membranes, J. Membr. Sci., 403–404 (2012) 101–109.
[65] H. Wu, B. Tang, P. Wu, Novel ultrafiltration membranes prepared from a multi-walled carbon nanotubes/polymer composite, J. Membr. Sci., 362 (2010) 374–383.
[66] B.D. McCloskey, H.B. Park, H. Ju, B.W. Rowe, D.J. Miller, B.J. Chun, K. Kin, B.D. Freeman, Influence of polydopamine deposition conditions on pure water flux and foulant adhesion resistance of reverse osmosis, ultrafiltration, and microfiltration membranes, Polymer, 51 (2010) 3472–3485.
[67] M.R. Esfahani, J.L. Tyler, H.A. Stretz, M.J.M. Wells, Effects of a dual nanofiller, nano-TiO_2 and MWCNT, for polysulfone-based nanocomposite membranes for water purification, Desalination, 372 (2015) 47–56.
[68] B. Yu, J. Liu, S. Liu, F. Zhou, Pdop layer exhibiting zwitterionicity: a simple electrochemical interface for governing ion permeability, Chem. Commun., 46 (2010) 5900–5902.
[69] A.K. Nair, A.M. Isloor, R. Kumar, A.F. Ismail, Antifouling and performance enhancement of polysulfone ultrafiltration membranes using $CaCO_3$ nanoparticles, Desalination, 322 (2013) 69–75.